Supplementary Information

Combined use of Residual Dipolar Couplings and Solution X-ray Scattering to Rapidly Probe Rigid Body Conformational Transitions in a Non-Phosphorylatable Active Site Mutant of the 128 kDa Enzyme I Dimer

Yuki Takayama,[1] Charles D. Schwieters,[2] Alexander Grishaev[1], Rodolfo Guirlando[3] and G. Marius Clore[1,]*

Laboratories of Chemical Physics[1] and Molecular Biology[3], National Institute of Diabetes and Digestive and Kidney Diseases, National Institutes of Health, Bethesda, Maryland 20892-0520 and [2]Division of Computational Bioscience, Center for Information and Technology, National Institutes of Health, Bethesda, MD 20892-5624

Experimental

The H189Q mutation was introduced into full length EI (residues 1-575) using the QuikChange mutagenesis kit (Stratagene). Cloning, expression, uniform $^{15}N/^{2}H$ isotopic labeling and purification of EI(H189Q) were identical to that previously described for wild-type EI.[S1] NMR samples comprised 0.15 mM U-[15N/2H]-EI(H189Q) dimer (0.3 mM in subunits) in 20 mM Tris buffer, pH 7.4, 100 mM NaCl, 10 mM dithiothreitol, 4 mM $MgCl_2$, 1 mM EDTA, 1 tablet of protease inhibitor cocktail (SigmaFast S8830) and 6% D2O (v/v). Samples for SAXS/WAXS were identical except that the concentration of EI(H189Q) dimer was 40 μM (80 μM in subunits).

NMR spectra were recorded at 37°C on a Bruker 600 MHz DRX spectrometer equipped with a *z*-shielded gradient triple resonance cryoprobe. Spectra were processed and analyzed using the programs NMRPipe[S2] and PIPP.[S3] Assignment of the EIN domain in the context of full-length EI(H189Q) was carried out only for the well-resolved cross-peaks in the 2D ^{1}H-^{15}N TROSY spectrum that overlayed directly onto well-resolved cross-peaks in the previously assigned spectrum of the isolated EIN domain,[S4] as described previously[S1] (See Fig. S1). $^{1}D_{NH}$ RDCs were measured by taking the difference in the one-bond ^{1}H-^{15}N splittings ($^{1}J_{NH} + {}^{1}D_{NH}$) in aligned (~11 mg/ml phage pf1[S5,S6]) and isotropic media using the TROSY-based ARTSY method.[S7]

SAXS/WAXS data collection at 25°C was exactly as described previously.[S1] The solution X-ray scattering data were acquired at the Beam Line 12-IDC at the Advanced Photon Source (Argonne National Laboratory, Argonne, IL) using a Gold CCD detector positioned at two distances, 4 m and 36 cm, corresponding to SAXS and WAXS, respectively.

Sedimentation velocity experiments to determine the dimerization constant for the EI(H189Q) dimer were performed and analyzed exactly as described previously for wild-type EI,[S1] and yielded a dimerization constant of 0.7 μM with 5-95% confidence limits of 0.5-0.8 μM. The values obtained for the Svedberg sedimentation coefficients (obtained by extrapolation to zero concentration) were 4.79 S and 5.74 S for the monomer and dimer, respectively. These values are similar to the values of 4.25 S and 5.68 S, respectively, obtained previously for wild-type EI.[S1] The concentration of monomer present in the NMR and SAXS/WAXS samples is very small, and model calculations indicate that the contribution of monomer to the RDC and SAXS/WAXS data is negligible (<5%) and can be ignored.

Isothermal titration calorimetry was performed using a MicroCal iTC 200 Microcalorimeter as described previously.[S1] The K_D for the binding of HPr to the EI(H189Q) mutant is 25±1 μM at 25°C and 11±2 μM at 37°C. These values are comparable to the values obtained for wild-type EI (29±1 μM and 7±2 μM),[S1] indicating that the H189Q mutation does not result in any significant perturbation in the interaction with HPr.

Simulated annealing refinement

The protocol used for conjoined rigid body/torsion angle/cartesian simulated annealing, which makes use of Xplor-NIH,[S8] was exactly as described for wild-type EI with the exception that the EIN^{α} and $EIN^{\alpha/\beta}$ subdomains were treated as separate rigid bodies with coordinate degrees of freedom given to the linker regions (residues 22-24 and 143-146) connecting the two subdomains. Detailed descriptions of the method used to calculate SAXS/WAXS curves and of the SAXS/WAXS restraint potential are provided in ref. S1. Structures were displayed using VMD-XPLOR.[S9]

Supplementary figures

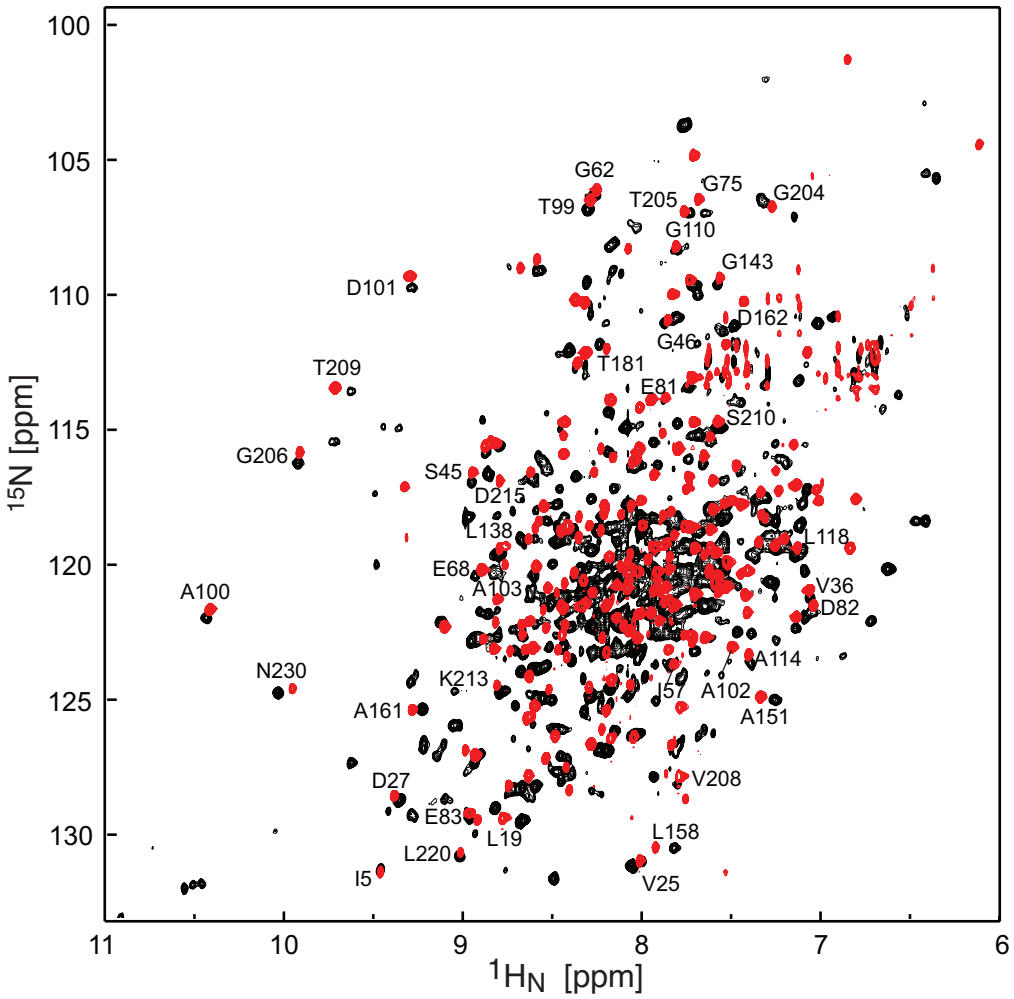

Figure S1. Overlay of ^{1}H-^{15}N TROSY spectrum of the intact (residues 1-575) *E. coli* E(H189Q) mutant and the isolated wild-type EIN (residues 1-249) domain (red) recorded at 600 MHz and 37°C. Clearly resolved cross-peaks in the EIN spectrum[S4] that are either not shifted or minimally shifted in the intact EI(H189Q) mutant are labeled.

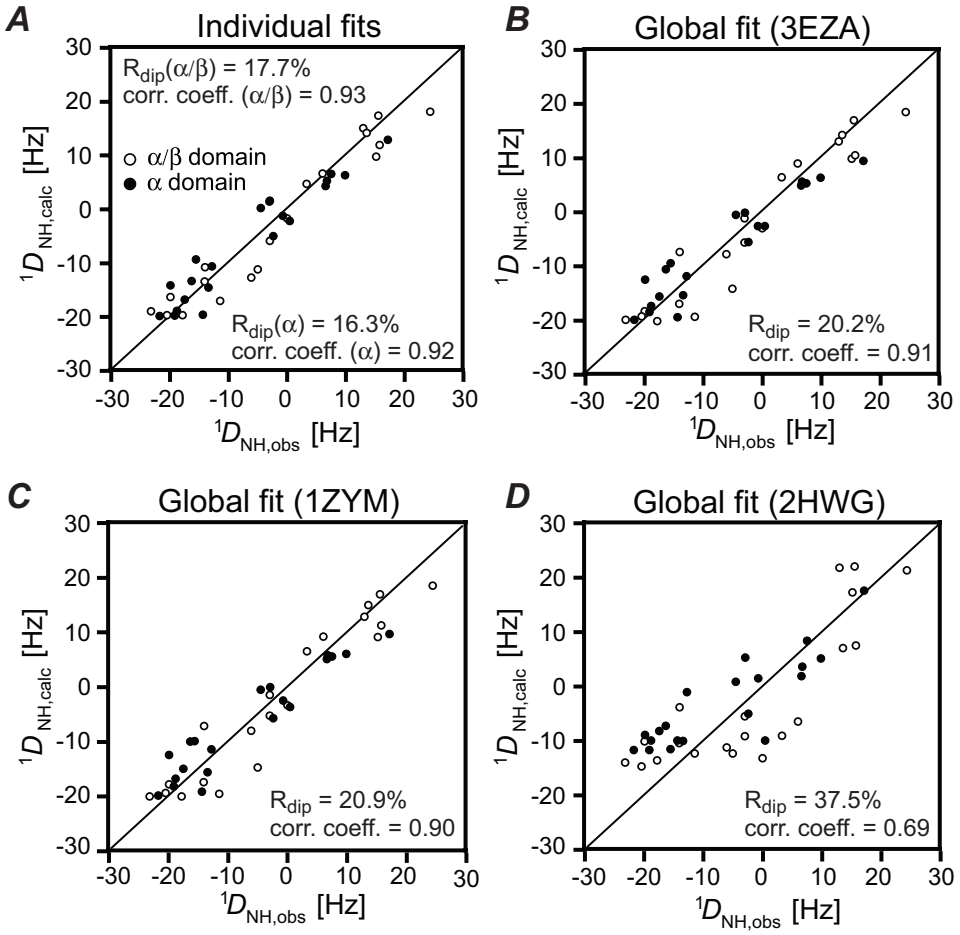

Figure S2. SVD analysis of the RDC data obtained for the EIN domain in the intact EI(H189Q) mutant. (A) SVD fits to the NMR coordinates (3EZA)[S10] of the EIN$^{\alpha}$ and EIN$^{\alpha/\beta}$ subdomains separately. Global fits to the whole EIN domain (single subunit) with the relative orientations of the EIN$^{\alpha}$ and EIN$^{\alpha/\beta}$ subdomains found in (B) the NMR structure of isolated EIN in the EIN-HPr complex (3EZA),[S10] (C) the X-ray structure of free isolated EIN (1ZYM)[S11] and (D) the X-ray structure of the EIN domain in the trapped phosphorylated intermediate of intact EI (2HWG).[S11] To ensure that the comparisons reflect only the relative orientations of the EIN$^{\alpha}$ and EIN$^{\alpha/\beta}$ subdomains and are not influenced by variations in atomic coordinates for the different structures, the NMR coordinates of isolated EIN (3EZA)[S10] are used throughout; the EIN$^{\alpha}$ and EIN$^{\alpha/\beta}$ subdomains are then best-fitted on to the X-ray coordinates of 1ZYM and 2HWG. The difference in the relative orientation of the EIN$^{\alpha}$ and EIN$^{\alpha/\beta}$ subdomains in 3EZA and 1ZYM is minimal (5.7°). All SVD analysis was carried out using Xplor-NIH.[S8]

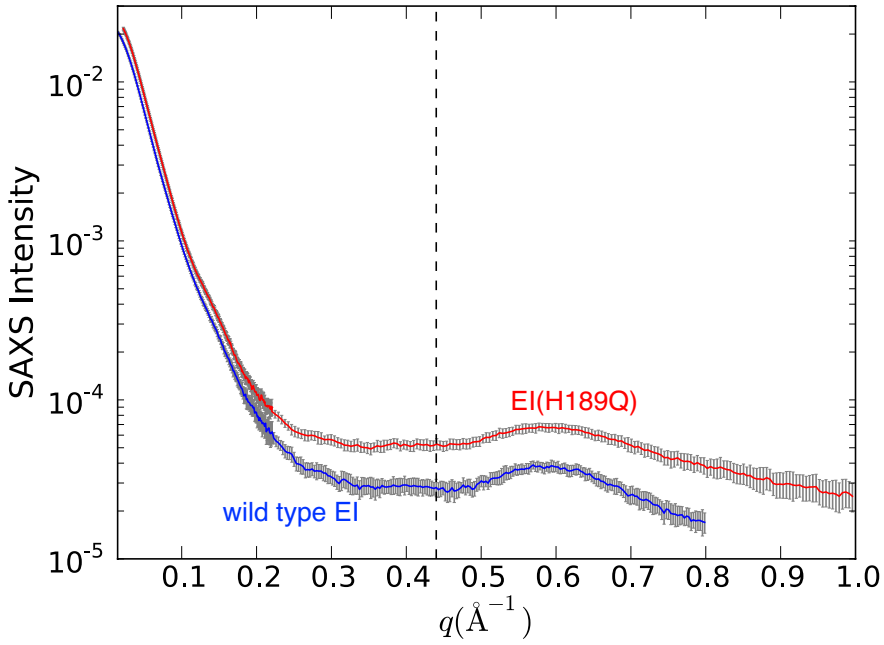

Figure S3. Comparison of SAXS/WAXS curves for the EI(H189Q) mutant (red) and wild type EI (blue). The two curves are offset for clarity, and the gray vertical error bars are equal to 1 s.d. The structures calculated in this paper and in the previous one on wild type EI[S1] were obtained by refining against the SAXS/WAXS data in the range $q \leq 0.44$ Å^{-1}, and the upper end of this range is indicated by the vertical dashed black line. The abrupt change in the magnitude of the error bars in the SAXS/WAXS curve at q = 0.22 Å^{-1} represents the change in geometry of the instrument from the SAXS (4 m detector distance) to WAXS (36 cm detector distance) regimes. The χ^2 values obtained upon fitting the restrained regularized mean structure of wild type EI to the wild type and mutant SAXS/WAXS data (up to $q \leq 0.44$ Å^{-1}) are 0.5 and 0.9, respectively. The χ^2 values obtained upon fitting the restrained regularized mean structure of the EI(H189Q) mutant to the wild type and mutant SAXS/WAXS data (up to $q \leq 0.44$ Å^{-1}) are 2.4 and 0.6, respectively. (Note that q_{max} for the SAXS regime is instrument dependent and the sizes of the commonly used detectors often dictate an associated q_{max} of 0.2 to 0.3 Å^{-1} which is generally considered to be the upper range of the SAXS regime and corresponds to interactomic interactions of 20-30 Å. Data up to q = 0.2-0.3 Å^{-1} can generally be relatively easily fitted by assuming a uniformly filled shape; this region often coincides with the fall-off of the main peak at q = 0.0 Å^{-1}, but that is size dependent and does not hold for large proteins or complex shapes such as the EI dimer).

Supplementary references

S1. Schwieters, C. D.; Suh, Y. J.; Grishaev, A.; Ghirlando, R., Takayama, Y. Clore, G.M. *J. Am. Chem. Soc.* **2010**, *132*, 13026-13045.

S2. Delaglio, F.; Grzesiek, S.; Vuister, G.; Zhu, G.; Pfeifer, J.; Bax, A. *J. Biomol. NMR* **1995**, *6*, 277-293.

S3. Garrett, D. S.; Powers, R.; Gronenborn, A. M.; Clore, G. M. *J. Magn. Reson.* **1991**, *95*, 214-220.

S4. Garrett, D. S., Seok, Y. K.; Liao, D. I.; Peterkofsky, A.; Gronenborn, A. M.; Clore, G. M. *Biochemistry* **1997**, *36*, 2517-2530.

S5. Clore, G. M.; Starich, M. A.; Gronenborn, A. M. *J. Am. Chem. Soc.* **1998**, *120*, 10571-10572.

S6. Hansen, M. R.; Mueller, L.; Pardi, A. *Nature Struct. Biol.* **1998**, *5*, 1065-1074.

S7. Fitzkee, N. C.; Bax, A. *J. Biomol. NMR* **2010**, *48*, 65-70.

S8. Schwieters, C. D.; Kuszewski, J.; Clore, G. M. *Progr. Nucl. Magn. Reson. Spectr.* **2006**, *48*, 57-62.

S9. Schwieters, C. D.; Clore, G. M. *J. Biomol. NMR* **2002**, *23*, 221-225.

S10. Garrett, D. S., Seok, Y. J.; Peterkofsky, A.; Gronenborn, A. M.; Clore, G. M. *Nature Struct. Biol.* **1999**, *6*, 166-173.

S11. Liao, D. I.; Silverton, E.; Seok,. Y. J., Lee, B. R.; Peterkofsky, A.; Davies, D. R. *Structure* **1996**, *4*, 861-872.

S12. Teplyakov, A.; Lim, K.; Zhu, P. P.; Kapadia, G.; Chen, C. C.; Schwatrz, J.; Howard, A.; Reddy, P. T.; Peterkofsky, A.; Herzberg, O. *Proc. Natl. Acad. Sci. U. S. A.* **2006**, *103*, 16218-16223.